MICROGRAVITY NUCLEATION AND PARTICLE COAGULATION EXPERIMENTS SUPPORT

Status Report II

For the Period June-November 1987

Submitted To

National Aeronautics and Space Administration
Goddard Space Flight Center
Greenbelt, Maryland 20771

For Work Performed under Grant NAG 5-865
by
Lembit U. Lilleleht and Frank T. Ferguson

Department of Chemical Engineering
School of Engineering and Applied Science
University of Virginia
Charlottesville, Virginia 22901

Report No. UVA/528260/CHE88/102

Copy No. _____

December 1987

Table of Contents

List of Figures

List of Tables

Executive Summary

This report summarizes our efforts on modeling the evolving temperature and concentration fields in the microgravity nucleation apparatus which is being fabricated and assembled at the NASA Goddard Space Flight Center. The report covers the period from 1 June through 30 November, 1987 and addresses the following major issues pertaining to the operation of the current design of the nucleation cloud chamber:

1. Time required to establish a steady temperature distribution;
2. Supersaturation ratios achievable during the 20-second microgravity periods available on KC-135; and
3. Power requirements for maintaining steady operating temperatures.

We have adapted the preliminary model for diffusion between concentric hemispheres to the cylindrical geometry of the apparatus under construction, and extended it to include the effects of radiation and conduction through the containment walls. Computer programs have been developed to calculate first the temperature distribution and then the evolving concentration field using a finite difference formulation of the trainsient diffusion and radiation processes.

The computational results summarized below assume the following:

- Cylindrical cloud chamber filled with Argon gas at 760 torr;
- Source of Magnesium vapors from the center of the top plate of the chamber at equilibrium vapor pressure corresponding to 1000K;
- Chamber bottom maintained as a constant temperature heat sink at 293K;
- Chamber side walls thermally insulated from the surroundings; and
- Criterion for steady temperature field: temperature changes at any grid point at a rate less than 0.05K/second.

For the above conditions, we estimate that:

1. It takes approximately 35 minutes to establish a steady temperature field;
2. Magnesium vapors released into the Argon environment at the "steady" temperature distribution will reach a maximum supersaturation ratio of approximately 10^4 in the 20-second period at a distance of 15 cm from the source of vapors;
3. Approximately 750W electrical power will be required to maintain "steady" operating temperatures within the chamber.

1 Introduction

The National Aeronautics and Space Administration (NASA) is currently studying the formation and interaction of fine-grained refractory particulates, and is planning a series of experiments to be carried out in a microgravity environment. These experiments will be used to determine under what conditions the vapors of refractory metals nucleate. The Chemical Engineering Department of the University of Virginia has undertaken to develop a mathematical model for this experiment, to assist in the apparatus design and construction phases, and to analyze the data once the experiments have begun. This report is a summary of the work at the University of Virginia on the modeling phase of the project.

Most of the research to date has been devoted to establishing the expected temperature and concentration fields in the cloud chamber of the experimental apparatus, a diagram of which is given in Figure 1.

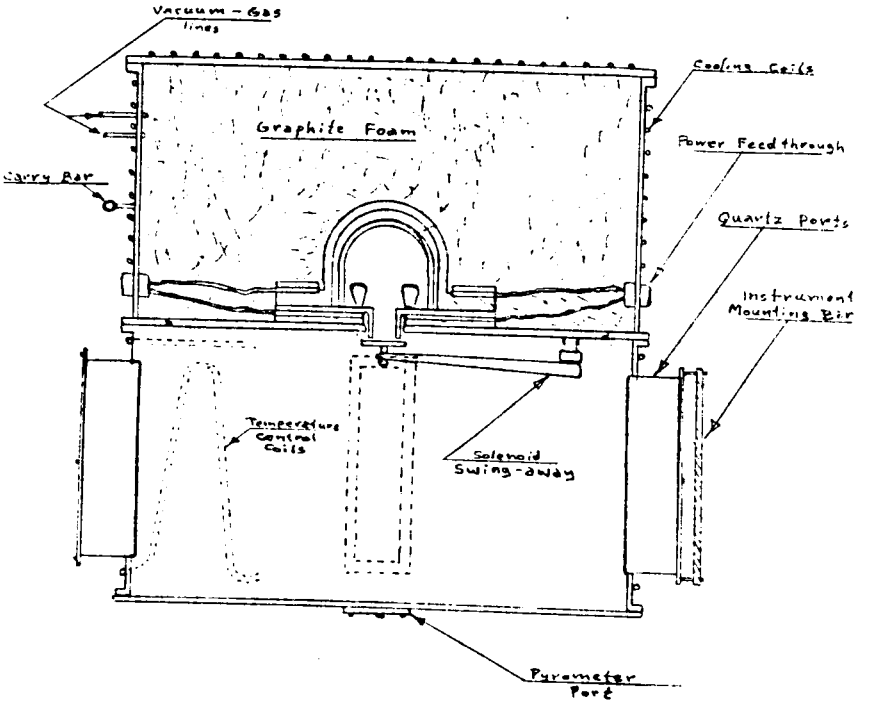

Figure 1: A Schematic of the Microgravity Nucleation Apparatus

The temperature distribution depends on the transport of energy by several different mechanisms, but in the particular design of Figure 1 it is expected to be influenced primarily by conduction and radiation. This report will address both the combined effects of these two mechanisms as well as look at their individual effects. The location in the

cloud chamber where nucleation and condensation condensation commence depends on the vapor supersaturation ratio. A plot of the logarithm of this supersaturation ratio is given for one of the most likely temperature distributions.

After initial laboratory tests, the experiment is expected to run aboard NASA's KC-135 aircraft wherein microgravity conditions can be produced for periods of approximately 20-30 seconds at a time. Since the power supplies in this aircraft are limited, the designer of the experiment needs to have an estimate of the amount of power required to run the experiment. A rough estimate of the power needed to maintain the experiment will also be given. These estimates of power requirements are based on the results from running the thermal model at the expected nucleation conditions.

2 The Temperature Distribution

The prediction of the temperature distribution in the experimental chamber is very important for a variety of reasons. The most obvious of these is that the supersaturation ratio is highly dependent on the temperature and that changes in the temperature can greatly affect the supersaturation profile. Also, the temperature distribution must be known to determine whether seals or other temperature sensitive components may be adversely affected by the high temperatures during the experiment. Finally, a knowledge of the temperature distribution and the mechanisms by which thermal energy is transferred are helpful in predicting the amount of energy required to maintain the experimental desired operating conditions.

In modeling the nucleation apparatus, several basic assumptions have been made about the chamber and its operation. First, the crucible heater and the bottom plate are considered to be isothermal and the temperatures of these two regions are usually taken to be 1000K and 293K respectively. The cloud chamber walls are considered to be adiabatic. Since the upper chamber will probably be insulated, this region is also considered to be adiabatic. The cloud chamber is assumed to be filled with pure, gaseous argon at a pressure of 760 torr and the diffusing metal is magnesium. Both the operating pressure and the diffusing species can easily be changed in the model.

This report deals with the transport of thermal energy through three paths:

- Conduction from the crucible heater through the ambient gas (argon) in the cloud chamber;

- Conduction from the crucible heater through the aluminum walls to the bottom of the chamber; and
- Radiation within the cloud chamber.

Methods of removing heat to maintain constant bottom temperatures and the effect of controlling the side wall temperature have not been studied as yet. These are topics for future research.

3 Conduction through Aluminum Wall

The crucible in the experimental apparatus will have to be maintained at very high temperatures. A significant amount of heat may be conducted through the aluminum plate that supports the crucible and down the side walls of the chamber. Such a flow of heat would lead to high temperatures along the plate and the wall, and could alter the temperature distribution within the chamber significantly. Since aluminum has a much higher thermal conductivity than argon, the walls of the chamber may tend to transfer thermal energy from the heater to the lower regions of the chamber. This conduction would not only increase the power losses but also tend to heat up regions in the lower part of the chamber. Cooler temperatures in the lower part are essential because they are necessary for high supersaturation ratios. Also, in the experimental chamber there is an O-ring between the top of the cloud chamber and the chamber walls. If the walls become too hot, the O-ring may become deformed and fail to seal the contents of the chamber. Figures 2 and 3 show the calculated steady state temperatures through the wall based on conduction alone.

Any heat conducted through the plate must flow through the O-ring, a seal between the plate and the walls of the chamber. Since the thermal conductivity of the O-ring is much lower than that of aluminum, there should be a large temperature drop across the O-ring at steady state. Figures 2 and 3 each show two curves--one which is based on the assumption of all-aluminum construction and one which accounts for the temperature drop across the O-ring. The O-ring was taken to be 3/16 of an inch (0.4763 cm) in diameter. Figures 2 and 3 show that there is indeed a large, approximately 660K, temperature drop across the O-ring. Such a thermal break would greatly reduce the heat flux along the wall and would keep the temperatures lower along the wall. Putting some type of break along the plate and/or the walls seems to be a reasonable and rather easy way of reducing the power requirements. Aluminum is very conductive and the apparatus would require a large amount of power if there was no break. Figures 2 and 3 also show that the temperature at the end of the plate near the O-ring would be extremely high, though, and would prob-

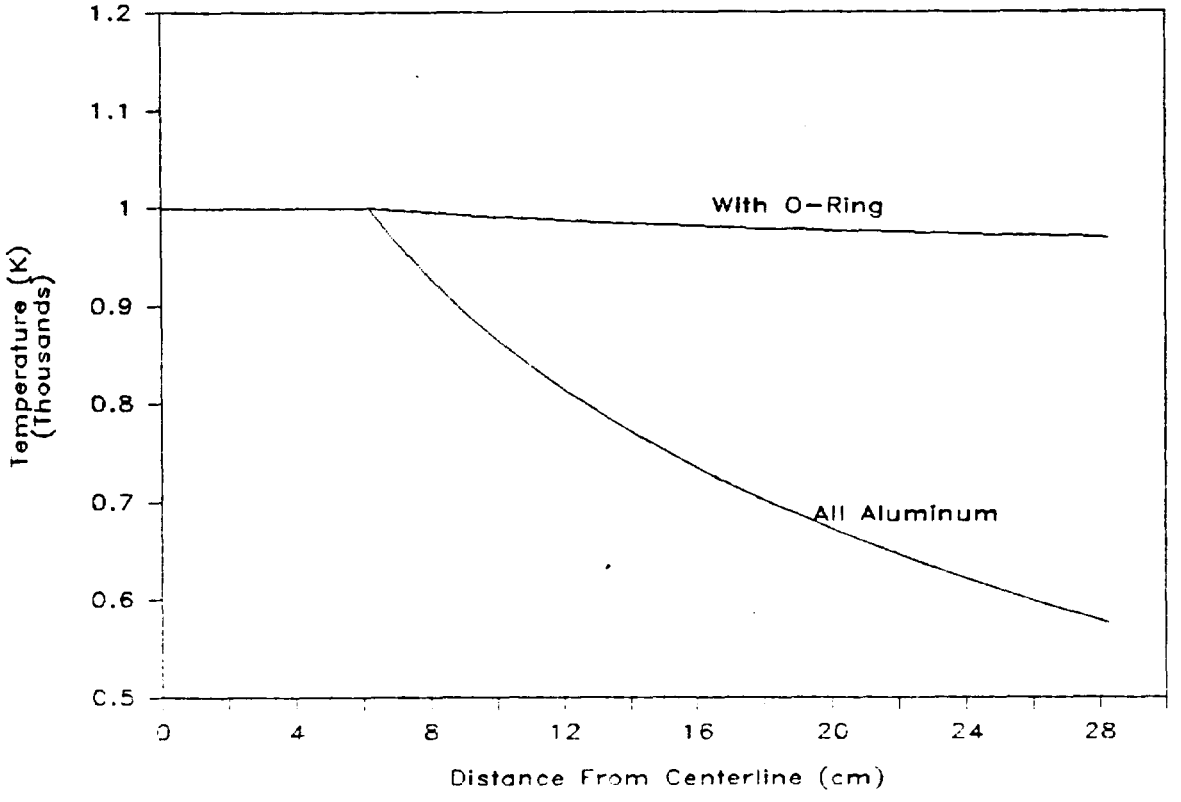

Figure 2: Top Plate Temperatures--Conduction through Aluminum Plate Only

ably be much higher than the thermal limits of the O-ring material. Even if the thermal break was not present, the temperatures in the top corner between the plate and the wall would still be very high. With all-aluminum walls, the predicted corner temperature is approximately 580K. All of these calculations are based on wall conduction alone independent of any other heat transfer mechanism. Radiation will certainly play a large role in determining the actual wall temperatures. Radiation will tend to cool down the top plate (which is very hot) and heat up the cooler regions in the bottom of the chamber. These effects are discussed in the next section.

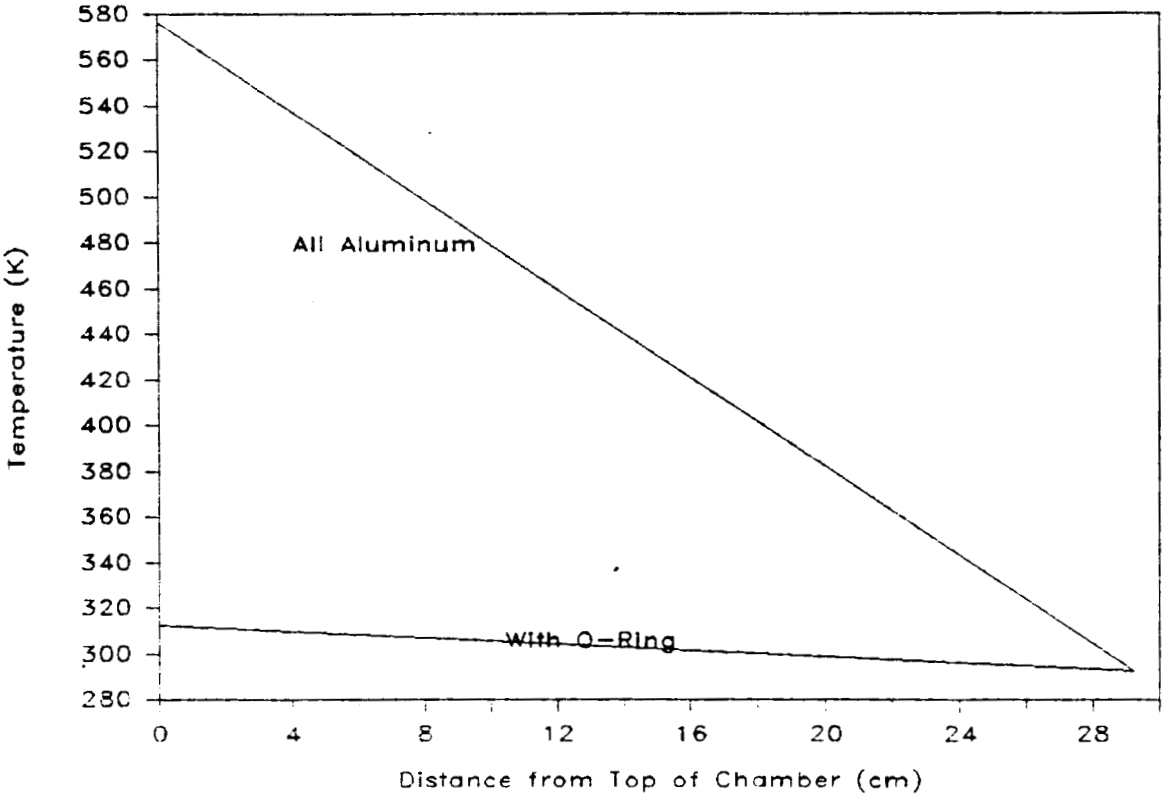

Figure 3: Wall Temperature Distribution

4 The Effect of Radiation within the Cloud Chamber

Heat transfer by radiation becomes very significant at high temperatures. Just as was pointed out for the wall conduction, radiation too can have a large effect on the temperature distribution as well as on how much power is needed for heating and cooling. Thermal radiation is described by the following formula:

$$q = -\epsilon\sigma F_{1-2} A(T_1^4 - T_2^4) \tag{1}$$

where q = net radiant heat flow
ϵ = emissivity
σ = Stefan-Boltzman constant = 5.672E-8 W/m^2-s
F_{1-2} = View Factor
A = Area of the radiating source
T_1, T_2 = Absolute temperatures of the source and the target, respectively

This equation permits the calculation of the net heat flow between two isothermal surfaces. It cannot be applied to the the radiant exchange in our situation since the walls of the cloud chamber will not be isothermal during the experiment. Therefore, the radiant transport is approximated by breaking the region within the chamber into a number of zones of constant temperature, and requires the solution of the following equation:

$$\sum_{j=1}^{n} \left(\frac{\delta_{kj}}{\epsilon_j} - \frac{1-\epsilon_j}{\epsilon_j}\right)\frac{Q_j}{A_j} = \sum_{j=1}^{n} (\delta_{kj} - F_{k-j})\sigma T_j^4 \qquad (2)$$

$$\delta_{kj} = \begin{cases} 1 & \text{if } k=j \\ 0 & \text{otherwise} \end{cases}$$

which relates the surface heating, Q, and the surface temperature, T, within an enclosure. In other words, the surface zones within the enclosure are either considered isothermal or adiabatic. Therefore Q is the amount of energy needed to keep a surface isothermal while T is the resulting steady state temperature of the adiabatic regions of the chamber wall. Figure 4 shows a diagram of the cloud chamber and the different zones.

Using Equation 2 with the six different zones gives a set of 4 simultaneous equations for the unknown temperatures which can easily be solved. After determining the view factors for the configuration of the cloud chamber and its zones, the various zone temperatures and heat duties were estimated using different emissivities. These results are presented in Table 1.

As shown in the table, radiation can have a great effect on the power requirements Also, it is apparent that this effect can be reduced by lower emissivity of the hot source. For an $\epsilon_1 = 1.0$, the heat duty is approximately 630 watts while it is only slightly more than 60 watts for an $\epsilon_1 = 0.1$. The temperature of the walls do not seem to be affected greatly by assuming different emissivities for these surfaces. Covering the top plate with a fine coating of low emissivity material, such as platinum for example, should greatly reduce the power losses due to radiation. Fortunately, the top plate is probably the only region where such a coating will be effective since the surfaces of other zones are expected to be

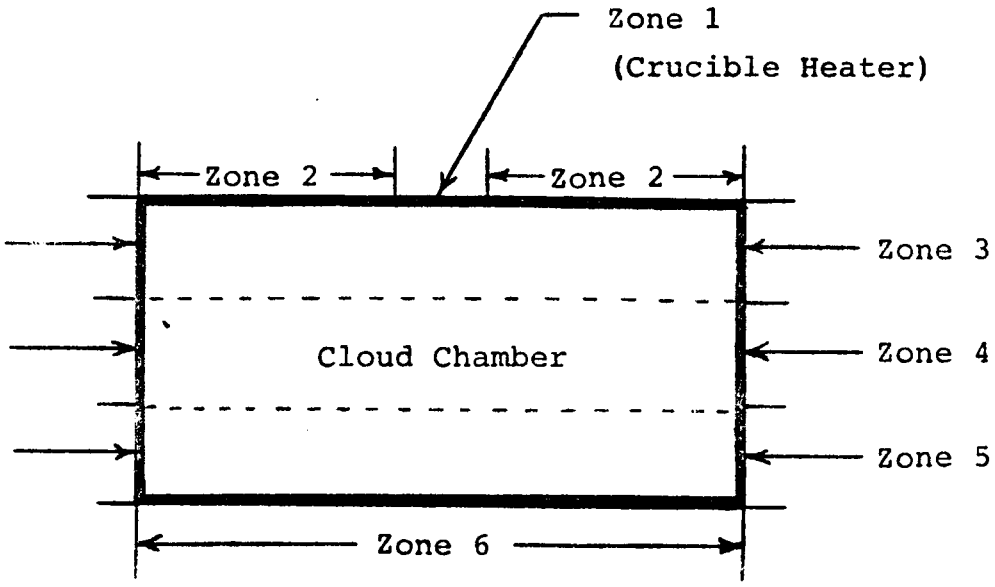

Figure 4: Zones used in Radiation Calculations

covered with condensed particulates during the experiment. The results of this analysis suggest that reducing the emissivities of the walls and the bottom are unnecessary anyway.

5 The Conduction through the Ambient Gas (Argon)

When the crucible heater is turned on and the temperature raised to 1000K or higher, the ambient argon gas will conduct heat throughout the cloud chamber. The ambient gas temperature is extremely important since this temperature greatly affects the supersaturation ratio. Figure 5 is a plot of the temperature distribution resulting from just the heat conduction mechanism through argon. This plot was made using numerical methods and represents the temperature distribution at steady state. In the plot, the bands are concentrated near the heater and most of the chamber is still relaively cool. Such a temperature distribution would probably give very high supersauration ratios since most of the temperature drop is concentrated around the heater area. Therefore, as the metal vapors diffuse from the crucible they would quickly reach low temperatures which would cause high supersaturation ratios.

Table 1: Radiation Results for Different Emissivities

All temperatures are in Kelvin
All duties are in Watts
Temperature of hot source T_1 = 1000K
Temperature of cold sink T_6 = 293K

ϵ_1	ϵ_2	Q_1	Q_6	T_2	T_3	T_4	T_5
0.1	0.1	62.2	-57.9	465	468	467	465
0.1	0.5	63.4	-63.9	344	352	351	345
0.1	1.0	63.6	-64.7	311	322	321	313
0.2	0.1	122	-112	538	542	541	538
0.2	0.5	126	-126	378	389	389	379
0.2	1.0	127	-128	326	344	343	329
0.3	0.1	179	-165	587	592	591	587
0.3	0.5	189	-188	404	418	418	406
0.3	1.0	190	-192	340	362	362	344
0.4	0.1	233	-215	625	630	629	625
0.4	0.5	251	-250	426	442	441	429
0.4	1.0	253	-255	351	378	378	356
0.5	0.1	286	-263	656	661	660	656
0.5	0.5	312	-310	445	462	462	448
0.5	1.0	316	-318	362	392	392	368
0.6	0.1	336	-309	682	688	686	682
0.6	0.5	373	-371	462	480	479	465
0.6	1.0	378	-380	376	404	404	378
0.7	0.1	385	-353	705	710	709	704
0.7	0.5	433	-431	477	496	495	480
0.7	1.0	441	-443	381	416	416	388
0.8	0.1	431	-395	724	730	729	724
0.8	0.5	493	-490	490	510	509	493
0.8	1.0	503	-505	389	426	427	397
0.9	0.1	476	-436	742	748	746	742
0.9	0.5	552	-549	502	523	523	506
0.9	1.0	565	-567	397	436	436	405
1.0	0.1	519	-476	758	764	762	758
1.0	0.5	611	-607	514	535	535	517
1.0	1.0	627	-629	404	445	446	413

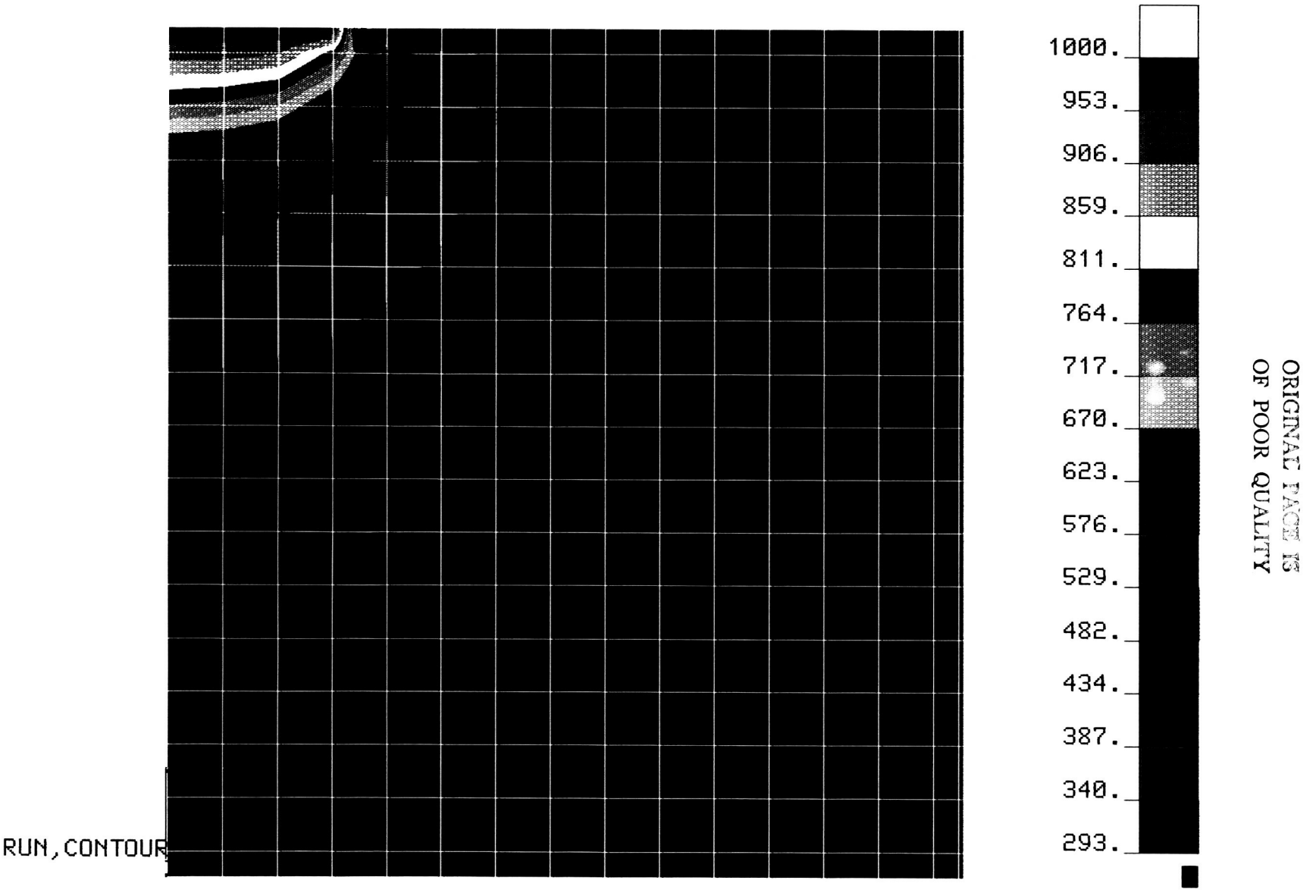

Figure 5: Temperature Distribution: Conduction through Argon Only

6 The Combined Effect of Conduction and Radiation

A program has also been developed which simulates the heating of the lower region of the experimental apparatus by the crucible heater. This program approximates the conduction of heat through the argon gas and the containing aluminum wall using finite difference approximations to the solution of the equation of energy. The effect of radiation is also accounted for by considering the zonal radiative flux over discrete time intervals. When the program runs, it calculates the temperature of different points in a gridwork over a certain time. During the next interval, it uses the data from the previous time interval to calculate new temperatures. This process continues until no temperature in the gridwork is changing faster than a rate of 0.05K per second. Figure 6 shows the temperature distribution from running the program with the following constraints:

- Zones 1 and 2 have emissivities of 0.1. Zones 3 through 6 have emissivities of 0.3 (Refer to Figure 4 for location of zones).
- The chamber walls (zones 3,4,5) are perfectly insulated from the outside environment.
- The bottom (zone 6) is kept isothermal at 293K.
- The region where the heater is located (zone 1), (the region between the centerline and 6 cm from the centerline), is kept isothermal at 1000K.

Figure 7 is a similar plot except the 6 zones all have emissivities of 1. Of the two plots, Figure 6 should be closer to the expected temperature distribution since the emissivities have more realistic values. The emissivity of the top plate was chosen approximately to equal the value of a platinum coating, while the other zones reflect emissivities close to that of highly oxidized aluminum. The temperature distribution in Figure 6 took approximately 35 minutes of simulation time, (which corresponds to 35 minutes of heating time), to reach our specification of steady state, i.e. less than 0.05K/s change in the temperatures at any grid point. Although the time to reach steady state was not calculated for the distribution in Figure 7, it should be comparable. Comparing the two plots, one sees that the temperature distribution along the centerline is approximately the same for both situations. Therefore, one would expect that the plots of the supersaturation ratios for these two temperature distributions would be similar in this region as well. Also, since nucleation is expected to occur first somewhere along the centerline, one would also expect that the point of highest supersaturation would be in the same general location even though the temperature distributions are definitely different. Figure 6 (lower

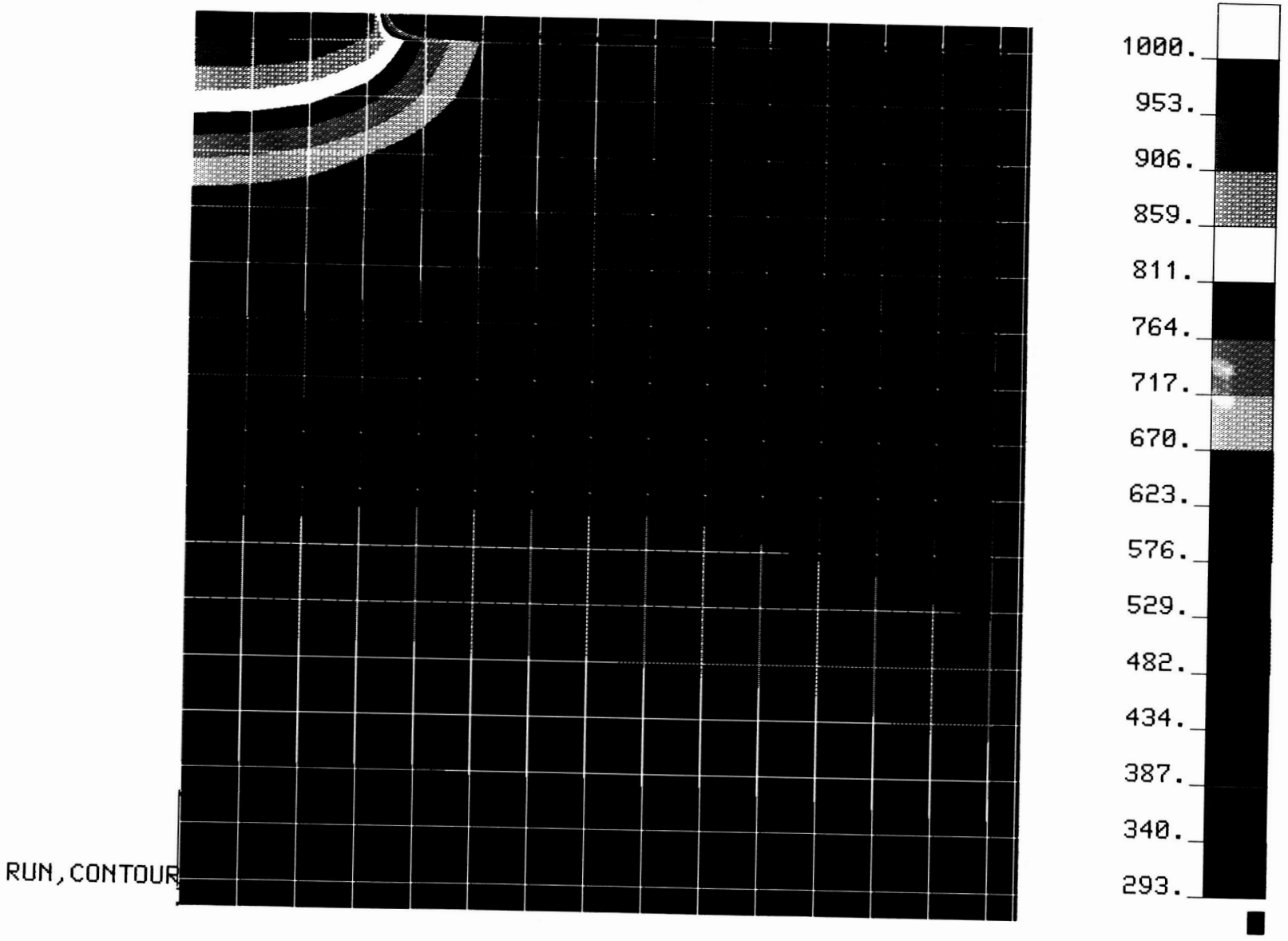

Figure 6: Temperature Distribution: Heater With Low Emissivity

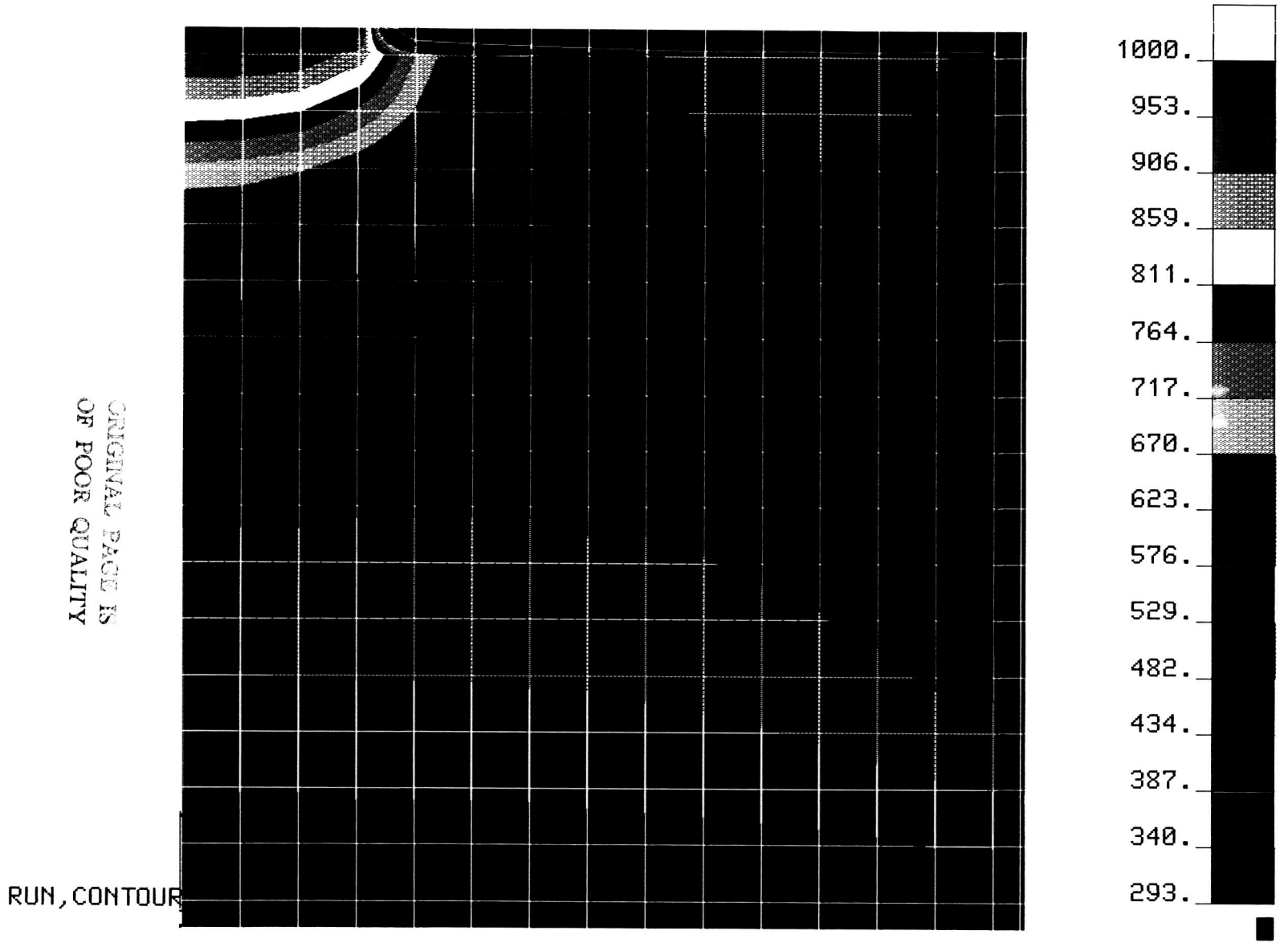

Figure 7: Temperature Distribution: Heater With High Emissivity

emissivities) has much higher temperatures along the top plate of the chamber than those of Figure 7. The model with the lower emissivities does not have the same ability to lose heat through radiation as the model with the higher emissivities. In fact, the model with the higher emissivities actually has a local minimum in the temperature which is probably due to a high radiative flux there. Therefore, the supersaturation plot based on the temperature distribution with the higher emissivities should also have a region of higher supersaturation ratios towards the corner of the chamber.

Since the temperature of the bottom plate is forced to remain at 293K, both temperature plots are expected to look similar along the lower part of the wall. The temperature distributions vary greatly along the upper part of the wall, however. In Figure 6, the heat transferred through radiation is smaller than in Figure 7. Therefore, conduction plays a larger role and the temperatures are higher than in Figure 7. In Figure 7 there is a broad, relatively hot band along the upper wall since the view factor between the hot source and this zone is large and the emissivities are at their maximum values. Altogether, the two plots should yield similar supersaturation plots except that the plot with lower emissivities should have the higher supersaturation ratios pushed closer to the centerline.

7 The Supersaturation Plots

Examples of the logarithm of the evolving supersaturation ratio for magnesium vapors corresponding to the two temperature plots are given in Figures 8 and 9. In addition, a supersaturation plot based on the temperature distribution of Figure 5, (conduction only through argon), is also given for comparison. The data for each of these plots were obtained from a program which simulates the transient diffusion of metal vapors within the nucleation chamber. Figure 8 is based on the temperature distribution where the emisssivities of the top plate are 0.1, (Figure 6), and Figure 9 is derived from the temperature distribution where the emissivities of all the regions within the chamber are 1.0, (Figure 7). Both of these plots are for a total elapsed time of 20 seconds from the first introduction of the vapors into the chamber. As expected, there are only small differences in the degree of supersaturation and the general shape of the supersaturation plots. Both plots have approximately the same maximum supersaturation ratio, and for both the point of highest supersaturation occurs about 14-15 cm down the centerline away from the heater. Figure 9, which is the plot based on the temperature distribution with all emisssivities equal to 1.0 also has a region of high supersaturation approximately 12 cm from the upper corner of the chamber. This local maximum in the supersaturation ratio occurs because

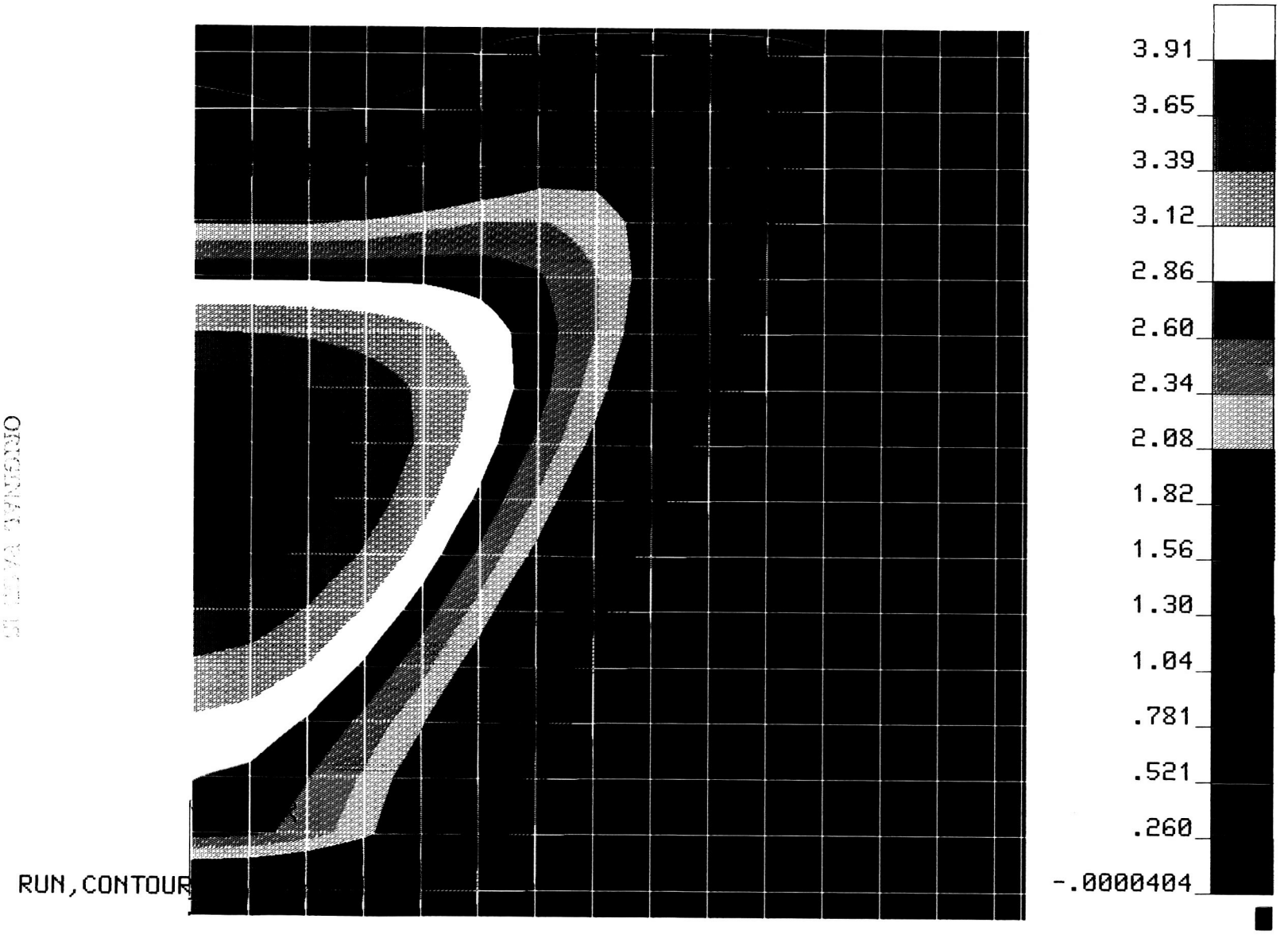

Figure 8: Supersaturation Plot--Based on Figure 6

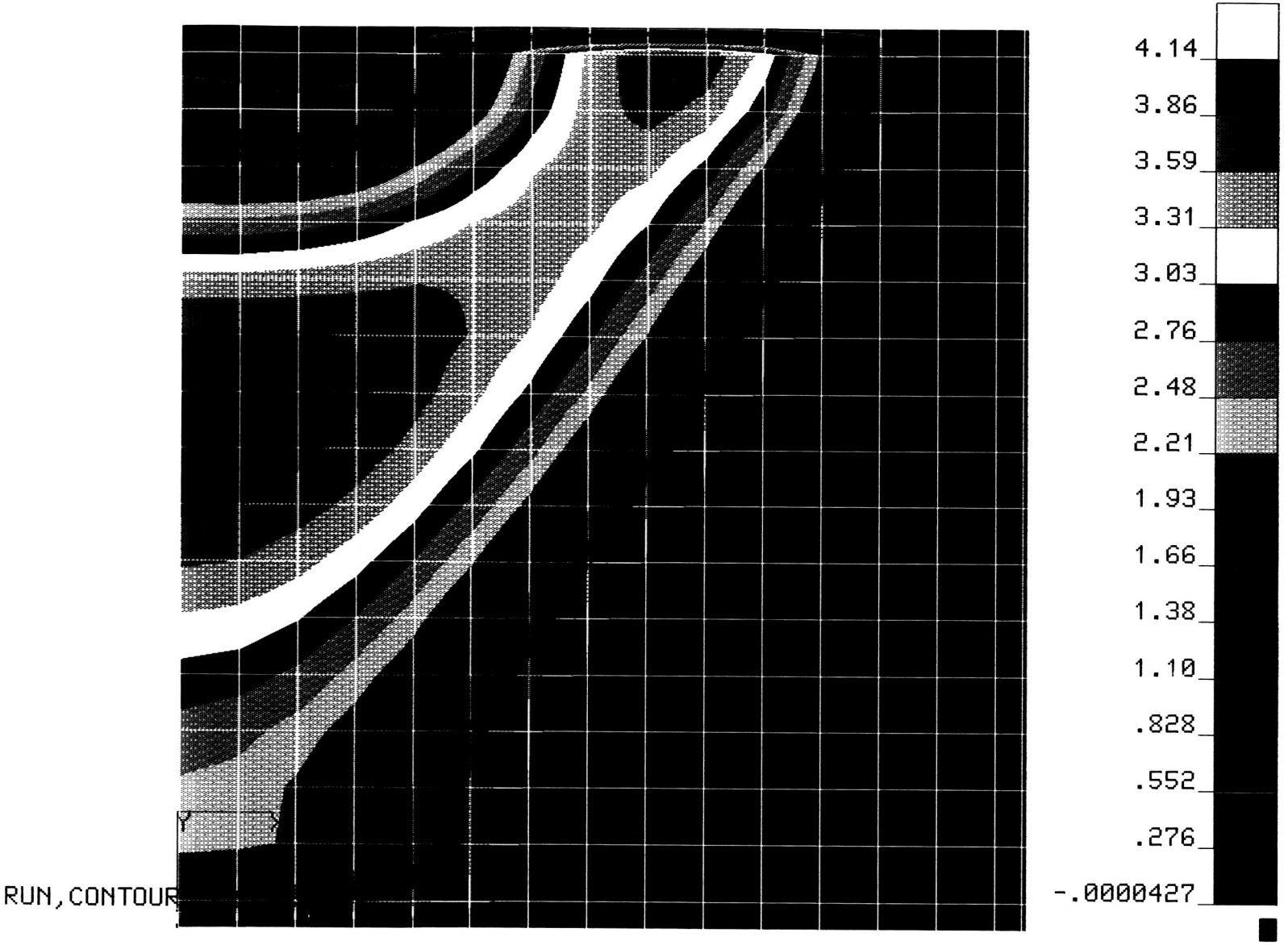

Figure 9: Supersaturation Plot--Based on Figure 7

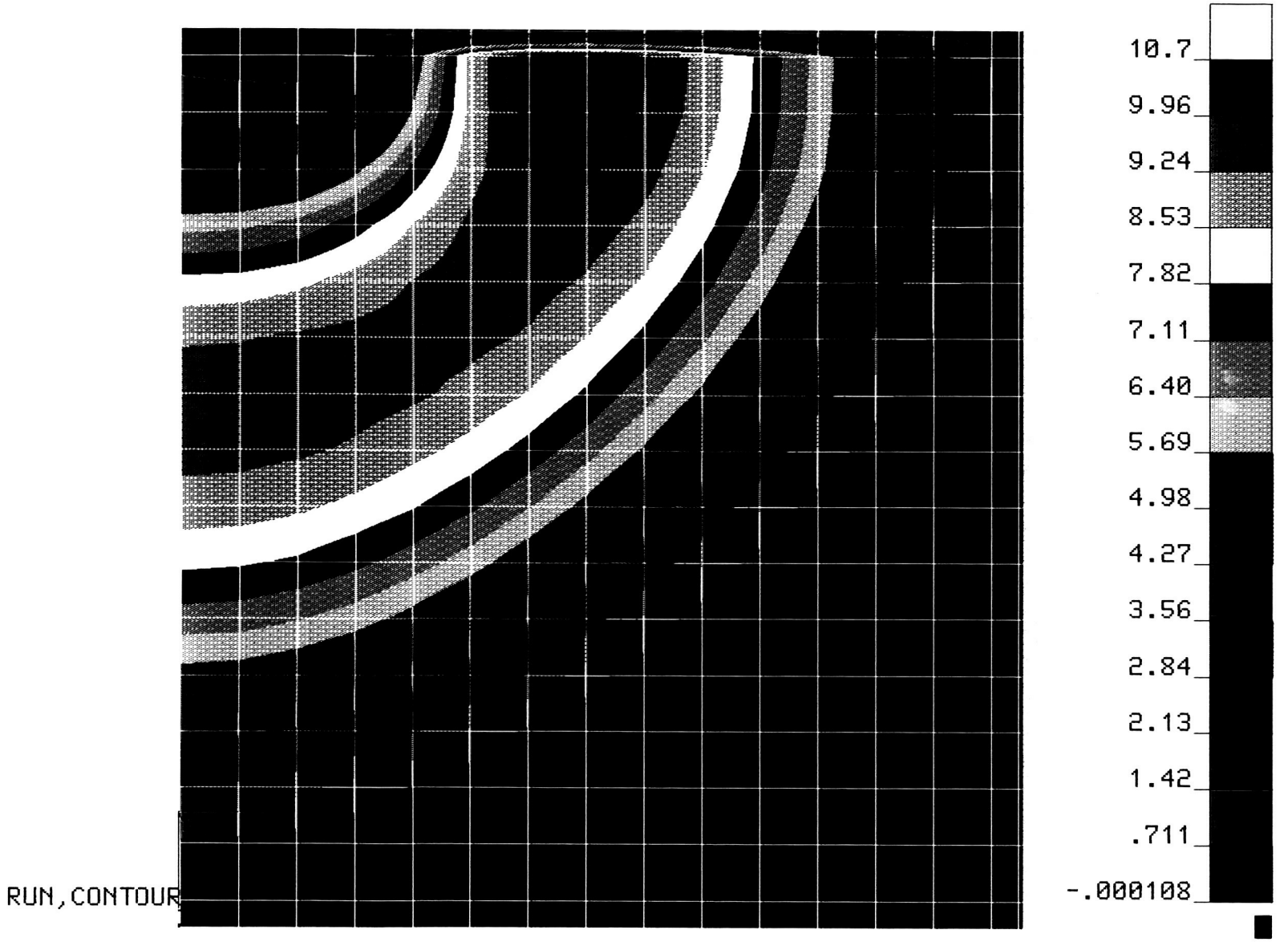

Figure 10: Supersaturation Plot--Based on Figure 5

radiation causes this region to be somewhat cooler and this increases the supersaturation ratio. Table 2 in Appendix I shows the evolution of supersaturation by listing the values of its logarithm at 5, 10, 15 and 20 seconds. Appendix II gives additional supersaturation plots based on these data.

8 Power Requirements

The power required to maintain the desired thermal conditions in the cloud chamber can be estimated from the calculated temperature distributions. One way of calculating the amount of power needed is to assume that the amount of energy supplied to the apparatus is equal to the energy lost or removed. In the mathematical model, the walls are considered to be adiabatic and the bottom plate is isothermal. The upper chamber is also considered to be adiabatic, and therefore, once heated to steady state temperatures, there should be no heat losses from this part. All of the heat losses from the cloud chamber are therefore considered to occur through the bottom plate.

An estimate of the total power needed to supply the heater can then be equated to the total power needed to maintain the bottom plate at 293K. Energy reaches the bottom plate by the three paths mentioned earlier--conduction through argon, conduction along the aluminum plate and wall, and radiation. Using data from the temperature model, the estimated values of each are:

Conduction through argon	=	17 watts
Conduction along wall	=	7,654 watts
Radiation	=	329 watts

which gives a total power requirement of approximately 8000 watts for the apparatus at steady state. This value is extremely high and would be unacceptable, if true. Estimated heat losses along the wall are probably much higher than they should be because the mathematical model which gives the temperature distribution considers the wall to be a contiguous piece of aluminum. In reality, there is an O-ring between the crucible plate and the chamber side walls which should act as a "thermal break" between the high temperatures of the upper plate and the cool region near the bottom plate. The effect of this thermal break was shown in Figures 2 and 3 with the steady state wall temperatures. The calculations used to derive these temperatures were based on the assumption of wall conduction only and did not consider the effect of radiation or loss of heat through argon. Nevertheless, the figures do show that there is a large temperature drop across the O-ring.

Neglecting radiation and argon conduction, the heat flux along the wall is only 237 watts. Although the heat flux along the wall may not be this low, because the wall conduction and radiation are coupled, the wall conduction is expected to be closer to this value than that of 7000 or 8000 watts mentioned above. Therefore, with an estimated upper wall conduction of approximately 400 watts, the total power requirement should be approximately 750 watts. These calculations again emphasize the need to reduce the heat flow along the wall with some type of a "thermal break."

9 Summary

A mathematical model based on finite difference methods has been developed which can simulate the transient temperature distribution in the microgravity nucleation cloud chamber now under construction at Goddard Space Flight Center. The program accounts not only for the conduction through the inert ambient gas (argon), but also for the effect of radiation within the enclosure, and the conduction along the aluminum side walls of the chamber. Once the temperature distribution has been established, the supersaturation ratios can be calculated from a somewhat similar program which models the transient diffusion of metal vapors. These programs can be used to predict evolving conditions within the chamber under different initial and boundary conditions.

A temperature distribution for one of the more likely sets of experimental conditions has been given in this report. These conditions are:

- Diffusion of magnesium vapors through argon atmostphere at a pressure of 760 torr from a hot source at 1000K with the bottom plate at 293K and with insulated side walls.
- The emissivity of the top plate equal to 0.1 and the emissivity of the walls and the bottom of the chamber equal to 0.3.

The temperature profile which corresponds to these conditions is estimated to take approximately 35 minutes to develop. The supersaturation profile is expected to reach a maximum of approximately 10^4 in 20 seconds at approximately 15 cm from the source of vapors in the top plate.

The steady state power requirements can be estimated from the temperature distributions. The losses by conduction through the argon atmosphere account for approximately 20 watts, and the losses due to radiaton in the cloud chamber are approximately 330

watts. The losses due to conduction along the heater plate and along the chamber wall to the bottom are more difficult to calculate. One calculation shows these losses to be quite large, but this estimate assumed no thermal break between the heater plate and the chamber walls. Such a break should greatly reduce the conductive heat flux from the heater through the chamber walls.

10 Areas for Future Research

The above results have pointed to areas of further research. One of these areas would be the refinement of the program which calculates the temperature distribution within the cloud chamber. This program should be modified to account for the thermal break(s) between the heater plate and the chamber walls. This would yield a better estimate of heat losses through the chamber walls and, in turn, improve the power requirement estimate. This program can then be used to predict the temperature distributions expected at different operating and boundary conditions. Although the program which calculates the transient diffusion of metal vapors does not seem to need any major improvements, it does need to be run to predict the behavior of other metals once the temperature distributions have been calculated.

Improvements of the temperature distribution model are also needed for determining where to place thermocouples. The location of a thermocouple depends on various factors. If a thermocouple is placed in a region where the temperature gradients are steep, then a small error in its placement may lead to large errors in the estimate of the temperature distribution. If the thermocouple is placed in a region where the gradients are less steep, say at the bottom or the sides, then the data may not be useful. Therefore, a compromise must be made between these two. Thermocouples should not be placed where they can have undue influence on the nucleation of the metal vapors. The diffusion model can predict where these positions are. Also, after the temperature distribution program is modified, it should also be able to provide a better estimate of the heating time required for the temperature distribution within the cloud chamber to reach steady state.

Another major area of further research should be to establish the influence of cooling the cloud chamber walls and bottom. Supersaturation profile depends heavily on the temperature distribution. Therefore, the method and intensity of cooling can affect both the shape of the supersaturation profile and the degree of supersaturation. The program which calculates the temperature distribution should be modified to accommodate cooling of the chamber walls, etc.

After the nucleation chamber is completed, experiments will be conducted in the laboratory at Goddard Space Flight Center. These experiments are expected to be affected by convection which may interfere with the uniform nucleation of particles. By conducting the experiments on the KC-135 in a microgravity environment, these problems are expected to be eliminated. Some calculations should be done to estimate whether this is a valid assumption, though. Modeling convection would involve the simultaneous solution of the temperature and velocity field within the chamber. This would probably be very difficult without making some simplifying assumptions. Nevertheless, the main question to be answered is whether convection will occur or not. Therefore, if a total solution of the temperature and velocity field cannot be obtained, perhaps at least it can be estimated whether convective effects will be significant or not.

I. Tabulated Transient Supersaturation Data

Table I-1: Diffusion of Magnesium in Argon

Temperature of Hot Source (K)	=	1000
Temperature of Cold Source (K)	=	293
Chamber Pressure (Torr)	=	760
Emissivity of Upper Plate	=	0.1
Emissivity of All Other Surfaces	=	0.3

When plotting the results, a represenative "slice" of the chamber is broken up into elements and numerical values are assigned to these elements. The table below gives temperature and supersaturation data as a function of the element number. A figure identifying the location of the various elements is given at the end of this table.

Element #	Temp (K)	Log Supersaturation Ratio			
		5 sec	10 sec	15 sec	20 sec
16	305.95080	0.0000000	0.0000000	0.2897084	2.7542233
17	305.98307	0.0000000	0.0000000	0.1075653	2.6199135
18	306.05009	0.0000000	0.0000000	0.0000000	2.3542047
19	306.16003	0.0000000	0.0000000	0.0000000	1.9619617
20	306.32388	0.0000000	0.0000000	0.0000000	1.4492574
21	306.55571	0.0000000	0.0000000	0.0000000	0.8226483
22	306.87265	0.0000000	0.0000000	0.0000000	0.0888156
23	307.29510	0.0000000	0.0000000	0.0000000	0.0000000
24	307.84825	0.0000000	0.0000000	0.0000000	0.0000000
25	308.56747	0.0000000	0.0000000	0.0000000	0.0000000
26	309.50640	0.0000000	0.0000000	0.0000000	0.0000000
27	310.72750	0.0000000	0.0000000	0.0000000	0.0000000
28	312.30841	0.0000000	0.0000000	0.0000000	0.0000000
29	314.35788	0.0000000	0.0000000	0.0000000	0.0000000
30	330.40490	0.0000000	0.0000000	0.6358048	2.7867995
31	330.48737	0.0000000	0.0000000	0.4603989	2.6558736
32	330.65990	0.0000000	0.0000000	0.1150047	2.3961619

table I-1, continued

33	330.94548	0.0000000	0.0000000	0.0000000	2.0108656
34	331.37501	0.0000000	0.0000000	0.0000000	1.5039894
35	331.98772	0.0000000	0.0000000	0.0000000	0.8797703
36	332.83050	0.0000000	0.0000000	0.0000000	0.1424609
37	333.95785	0.0000000	0.0000000	0.0000000	0.0000000
38	335.43262	0.0000000	0.0000000	0.0000000	0.0000000
39	337.33252	0.0000000	0.0000000	0.0000000	0.0000000
40	339.81829	0.0000000	0.0000000	0.0000000	0.0000000
41	343.04181	0.0000000	0.0000000	0.0000000	0.0000000
42	347.18695	0.0000000	0.0000000	0.0000000	0.0000000
43	352.47281	0.0000000	0.0000000	0.0000000	0.0000000
44	353.17344	0.0000000	0.0000000	1.1240950	2.9712858
45	353.27747	0.0000000	0.0000000	0.9568113	2.8454263
46	353.50048	0.0000000	0.0000000	0.6262952	2.5951019
47	353.87911	0.0000000	0.0000000	0.1385603	2.2222363
48	354.46337	0.0000000	0.0000000	0.0000000	1.7291736
49	355.31567	0.0000000	0.0000000	0.0000000	1.1183228
50	356.50903	0.0000000	0.0000000	0.0000000	0.3921021
51	358.12655	0.0000000	0.0000000	0.0000000	0.0000000
52	360.26251	0.0000000	0.0000000	0.0000000	0.0000000
53	363.03000	0.0000000	0.0000000	0.0000000	0.0000000
54	366.62812	0.0000000	0.0000000	0.0000000	0.0000000
55	371.26097	0.0000000	0.0000000	0.0000000	0.0000000
56	377.18971	0.0000000	0.0000000	0.0000000	0.0000000
57	384.79395	0.0000000	0.0000000	0.0000000	0.0000000
58	374.77734	0.0000000	0.0000000	1.6608901	3.2181038
59	374.86495	0.0000000	0.0000000	1.5029333	3.0987432
60	375.06484	0.0000000	0.0000000	1.1898548	2.8607055
61	375.42909	0.0000000	0.0000000	0.7257844	2.5047791
62	376.02897	0.0000000	0.0000000	0.1151419	2.0317892
63	376.95124	0.0000000	0.0000000	0.0000000	1.4424772
64	378.29422	0.0000000	0.0000000	0.0000000	0.7376354
65	380.16613	0.0000000	0.0000000	0.0000000	0.0000000
66	382.68729	0.0000000	0.0000000	0.0000000	0.0000000
67	385.99909	0.0000000	0.0000000	0.0000000	0.0000000
68	390.27816	0.0000000	0.0000000	0.0000000	0.0000000
69	395.73975	0.0000000	0.0000000	0.0000000	0.0000000
70	402.66767	0.0000000	0.0000000	0.0000000	0.0000000
71	411.46317	0.0000000	0.0000000	0.0000000	0.0000000
72	395.55358	0.0000000	0.0000000	2.1907978	3.4739349
73	395.57245	0.0000000	0.0000000	2.0435376	3.3626187
74	395.64989	0.0000000	0.0000000	1.7506503	3.1398819
75	395.85795	0.0000000	0.0000000	1.3144966	2.8053973
76	396.29542	0.0000000	0.0000000	0.7372467	2.3584138
77	397.07862	0.0000000	0.0000000	0.0207146	1.7979361
78	398.33343	0.0000000	0.0000000	0.0000000	1.1231104

table I-1, continued

79	400.19030	0.0000000	0.0000000	0.0000000	0.3336326
80	402.78342	0.0000000	0.0000000	0.0000000	0.0000000
81	406.25440	0.0000000	0.0000000	0.0000000	0.0000000
82	410.75927	0.0000000	0.0000000	0.0000000	0.0000000
83	416.47902	0.0000000	0.0000000	0.0000000	0.0000000
84	423.64531	0.0000000	0.0000000	0.0000000	0.0000000
85	432.60810	0.0000000	0.0000000	0.0000000	0.0000000
86	415.88872	0.0000000	0.8324890	2.6731040	3.7005869
87	415.76563	0.0000000	0.6258207	2.5382562	3.5991439
88	415.58371	0.0000000	0.2191118	2.2689015	3.3952048
89	415.44456	0.0000000	0.0000000	1.8656015	3.0872252
90	415.48744	0.0000000	0.0000000	1.3280540	2.6726281
91	415.87021	0.0000000	0.0000000	0.6554550	2.1483775
92	416.75452	0.0000000	0.0000000	0.0000000	1.5117029
93	418.29547	0.0000000	0.0000000	0.0000000	0.7608104
94	420.63682	0.0000000	0.0000000	0.0000000	0.0000000
95	423.91090	0.0000000	0.0000000	0.0000000	0.0000000
96	428.24116	0.0000000	0.0000000	0.0000000	0.0000000
97	433.74491	0.0000000	0.0000000	0.0000000	0.0000000
98	440.53140	0.0000000	0.0000000	0.0000000	0.0000000
99	448.66797	0.0000000	0.0000000	0.0000000	0.0000000
100	436.40309	0.0000000	1.6144031	3.0699861	3.8632785
101	436.03172	0.0000000	1.4285905	2.9498092	3.7740036
102	435.39441	0.0000000	1.0607745	2.7083258	3.5932196
103	434.64074	0.0000000	0.5159233	2.3441310	3.3179510
104	433.97505	0.0000000	0.0000000	1.8539727	2.9433157
105	433.62001	0.0000000	0.0000000	1.2338053	2.4636443
106	433.79061	0.0000000	0.0000000	0.4801135	1.8736860
107	434.67654	0.0000000	0.0000000	0.0000000	1.1697192
108	436.43414	0.0000000	0.0000000	0.0000000	0.3502755
109	439.18512	0.0000000	0.0000000	0.0000000	0.0000000
110	443.01832	0.0000000	0.0000000	0.0000000	0.0000000
111	447.98880	0.0000000	0.0000000	0.0000000	0.0000000
112	454.10567	0.0000000	0.0000000	0.0000000	0.0000000
113	461.29053	0.0000000	0.0000000	0.0000000	0.0000000
114	458.07423	0.0000000	2.2419383	3.3431190	3.9272525
115	457.29255	0.0000000	2.0797883	3.2406078	3.8530842
116	455.90455	0.0000000	1.7565436	3.0327837	3.7010899
117	454.14203	0.0000000	1.2732222	2.7160065	3.4665801
118	452.31948	0.0000000	0.6268953	2.2832773	3.1416011
119	450.76663	0.0000000	0.0000000	1.7262653	2.7168621
120	449.78305	0.0000000	0.0000000	1.0375054	2.1836970
121	449.61100	0.0000000	0.0000000	0.2122233	1.5357373
122	450.42657	0.0000000	0.0000000	0.0000000	0.7698996
123	452.34266	0.0000000	0.0000000	0.0000000	0.0000000
124	455.41668	0.0000000	0.0000000	0.0000000	0.0000000

table I-1, continued

125	459.65674	0.0000000	0.0000000	0.0000000	0.0000000
126	465.02255	0.0000000	0.0000000	0.0000000	0.0000000
127	471.42084	0.0000000	0.0000000	0.0000000	0.0000000
128	482.43506	0.6111147	2.6672997	3.4517728	3.8556934
129	480.98516	0.2914280	2.5326089	3.3706851	3.8002250
130	478.37978	0.0000000	2.2617842	3.2040750	3.6842176
131	474.99513	0.0000000	1.8517697	2.9458748	3.5011034
132	471.33870	0.0000000	1.2928388	2.5841169	3.2387121
133	467.92301	0.0000000	0.5728187	2.1045000	2.8825299
134	465.18394	0.0000000	0.0000000	1.4940661	2.4189992
135	463.44127	0.0000000	0.0000000	0.7439609	1.8380687
136	462.89634	0.0000000	0.0000000	0.0000000	1.1344550
137	463.64950	0.0000000	0.0000000	0.0000000	0.3077909
138	465.72211	0.0000000	0.0000000	0.0000000	0.0000000
139	469.07634	0.0000000	0.0000000	0.0000000	0.0000000
140	473.63247	0.0000000	0.0000000	0.0000000	0.0000000
141	479.28835	0.0000000	0.0000000	0.0000000	0.0000000
142	511.89738	1.4142727	2.8391975	3.3533356	3.6097452
143	509.35899	1.1520816	2.7360968	3.2974971	3.5765219
144	504.77307	0.6487699	2.5273908	3.1810129	3.5048349
145	498.76944	0.0000000	2.2063917	2.9958925	3.3868382
146	492.20516	0.0000000	1.7545536	2.7233905	3.2044669
147	485.91629	0.0000000	1.1491606	2.3403954	2.9352515
148	480.55867	0.0000000	0.3709690	1.8260077	2.5583661
149	476.55621	0.0000000	0.0000000	1.1658093	2.0586312
150	474.12771	0.0000000	0.0000000	0.3532543	1.4279260
151	473.33979	0.0000000	0.0000000	0.0000000	0.6648988
152	474.15520	0.0000000	0.0000000	0.0000000	0.0000000
153	476.46894	0.0000000	0.0000000	0.0000000	0.0000000
154	480.13677	0.0000000	0.0000000	0.0000000	0.0000000
155	485.00909	0.0000000	0.0000000	0.0000000	0.0000000
156	550.25518	1.8254244	2.7101201	3.0092739	3.1535560
157	545.95630	1.6213701	2.6399909	2.9794839	3.1429868
158	538.13168	1.2328053	2.5021087	2.9205470	3.1222688
159	527.83515	0.6598054	2.2890291	2.8256900	3.0856168
160	516.58727	0.0000000	1.9702858	2.6665828	3.0064438
161	505.83216	0.0000000	1.5070636	2.4059834	2.8491084
162	496.57950	0.0000000	0.8667939	2.0109660	2.5814864
163	489.36485	0.0000000	0.0301124	1.4595718	2.1813163
164	484.37639	0.0000000	0.0000000	0.7416535	1.6370792
165	481.59017	0.0000000	0.0000000	0.0000000	0.9465459
166	480.86190	0.0000000	0.0000000	0.0000000	0.1147598
167	481.97826	0.0000000	0.0000000	0.0000000	0.0000000
168	484.68469	0.0000000	0.0000000	0.0000000	0.0000000
169	488.70180	0.0000000	0.0000000	0.0000000	0.0000000
170	603.32295	1.7943066	2.2575507	2.4033551	2.4712602

table I-1, continued

171	596.32361	1.6373459	2.2087447	2.3871404	2.4703969
172	583.28124	1.3642177	2.1395876	2.3820824	2.4961283
173	565.82297	0.9749423	2.0524226	2.3936955	2.5561322
174	546.83493	0.4148071	1.8993556	2.3788230	2.6102269
175	529.03434	0.0000000	1.6136802	2.2744249	2.5979829
176	513.98514	0.0000000	1.1423328	2.0284697	2.4689019
177	502.24732	0.0000000	0.4555269	1.6092268	2.1914061
178	493.82736	0.0000000	0.0000000	1.0028368	1.7504578
179	488.48666	0.0000000	0.0000000	0.2087963	1.1433771
180	485.89052	0.0000000	0.0000000	0.0000000	0.3764495
181	485.66336	0.0000000	0.0000000	0.0000000	0.0000000
182	487.39997	0.0000000	0.0000000	0.0000000	0.0000000
183	490.66353	0.0000000	0.0000000	0.0000000	0.0000000
184	679.24068	1.3437419	1.5275394	1.5811332	1.6052024
185	668.75351	1.1844802	1.4487619	1.5261851	1.5612426
186	647.96654	0.9913809	1.4099590	1.5353861	1.5932011
187	618.42212	0.7955660	1.4549091	1.6587877	1.7548099
188	586.15300	0.5052323	1.5072970	1.8274059	1.9813349
189	557.06765	0.0000000	1.4424014	1.9221384	2.1572315
190	533.45460	0.0000000	1.1752982	1.8604067	2.2021182
191	515.46363	0.0000000	0.6649588	1.5999074	2.0742652
192	502.53512	0.0000000	0.0000000	1.1242352	1.7562754
193	493.97991	0.0000000	0.0000000	0.4332648	1.2458170
194	489.14741	0.0000000	0.0000000	0.0000000	0.5506942
195	487.43972	0.0000000	0.0000000	0.0000000	0.0000000
196	488.27305	0.0000000	0.0000000	0.0000000	0.0000000
197	491.02496	0.0000000	0.0000000	0.0000000	0.0000000
198	786.65352	0.6515588	0.6961657	0.7082121	0.7134417
199	774.06383	0.3423918	0.4371737	0.4634743	0.4750904
200	745.15738	0.1013157	0.3016340	0.3601953	0.3868607
201	694.85251	0.0763060	0.4589689	0.5770662	0.6325862
202	638.36884	0.1079487	0.7720346	0.9864412	1.0899833
203	591.20824	0.0000000	0.9754203	1.3299883	1.5050243
204	555.31834	0.0000000	0.9457403	1.4877227	1.7604480
205	529.01087	0.0000000	0.6356066	1.4116294	1.8091915
206	510.35508	0.0000000	0.0334788	1.0861698	1.6349284
207	497.84121	0.0000000	0.0000000	0.5122948	1.2364032
208	490.34586	0.0000000	0.0000000	0.0000000	0.6223202
209	486.99930	0.0000000	0.0000000	0.0000000	0.0000000
210	487.04883	0.0000000	0.0000000	0.0000000	0.0000000
211	489.69750	0.0000000	0.0000000	0.0000000	0.0000000
212	925.53515	0.0942126	0.0979963	0.0989670	0.0993802
213	918.67450	0.0000000	0.0000000	0.0000000	0.0000000
214	897.29100	0.0000000	0.0000000	0.0000000	0.0000000
215	811.37228	0.0000000	0.0000000	0.0000000	0.0000000
216	705.78869	0.0000000	0.0000000	0.0000000	0.0000000

table I-1, continued

217	631.18135	0.0000000	0.1798807	0.4606617	0.6007392
218	579.08433	0.0000000	0.4020219	0.8571998	1.0886516
219	542.47045	0.0000000	0.3040243	0.9818891	1.3327398
220	516.90058	0.0000000	0.0000000	0.8231719	1.3209180
221	499.64694	0.0000000	0.0000000	0.3818187	1.0518231
222	488.97617	0.0000000	0.0000000	0.0000000	0.5325126
223	483.72763	0.0000000	0.0000000	0.0000000	0.0000000
224	483.06184	0.0000000	0.0000000	0.0000000	0.0000000
225	486.25889	0.0000000	0.0000000	0.0000000	0.0000000
Supersaturation Maxima-->		1.8254244	2.8391975	3.4517728	3.9272525

212	213	214	215	216	217	218	219	220	221	222	223	224	225
198	199	200	201	202	203	204	205	206	207	208	209	210	211
184	185	186	187	188	189	190	191	192	193	194	195	196	197
170	171	172	173	174	175	176	177	178	179	180	181	182	183
156	157	158	159	160	161	162	163	164	165	166	167	168	169
142	143	144	145	146	147	148	149	150	151	152	153	154	155
128	129	130	131	132	133	134	135	136	137	138	139	140	141
114	115	116	117	118	119	120	121	122	123	124	125	126	127
100	101	102	103	104	105	106	107	108	109	110	111	112	113
86	87	88	89	90	91	92	93	94	95	96	97	98	99
72	73	74	75	76	77	78	79	80	81	82	83	84	85
58	59	60	61	62	63	64	65	66	67	68	69	70	71
44	45	46	47	48	49	50	51	52	53	54	55	56	57
30	31	32	33	34	35	36	37	38	39	40	41	42	43
16	17	18	19	20	21	22	23	24	25	26	27	28	29

Figure I-1: Element Location for Temperature and Supersaturation Plots

II. Transient Supersaturation Plots

The following pages give the transient supersaturation plots for the diffusion of magnesium in an argon atmosphere at 760 torr. These supersaturation plots are based on the temperature distribution given in Figure 6. The plots are given for 5, 10, and 15 seconds and a plot of the supersaturation profile at 20 seconds is given in Figure 8.

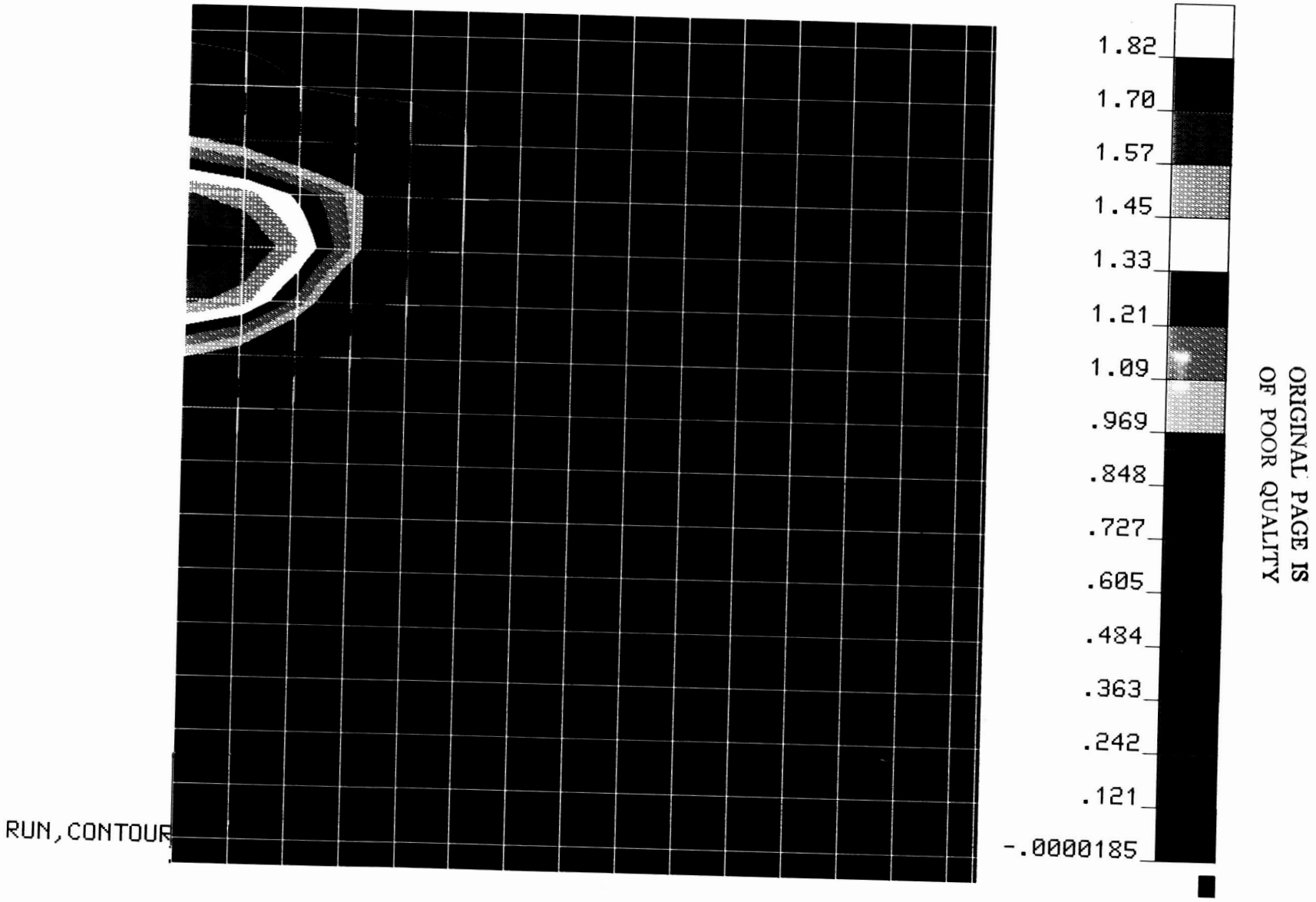

Figure II-1: Supersaturation Profile at 5 seconds

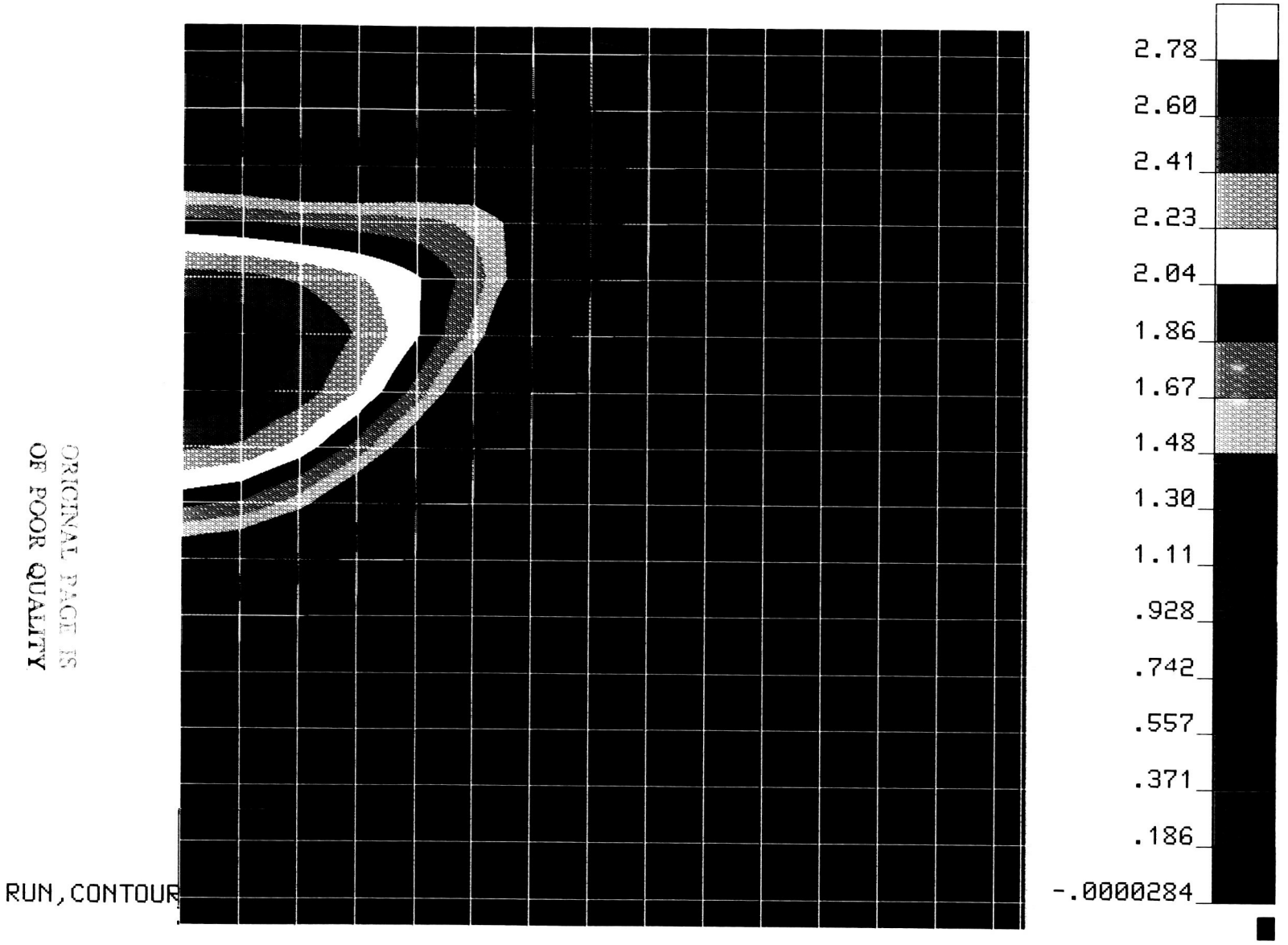

Figure II-2: Supersaturation Profile at 10 seconds

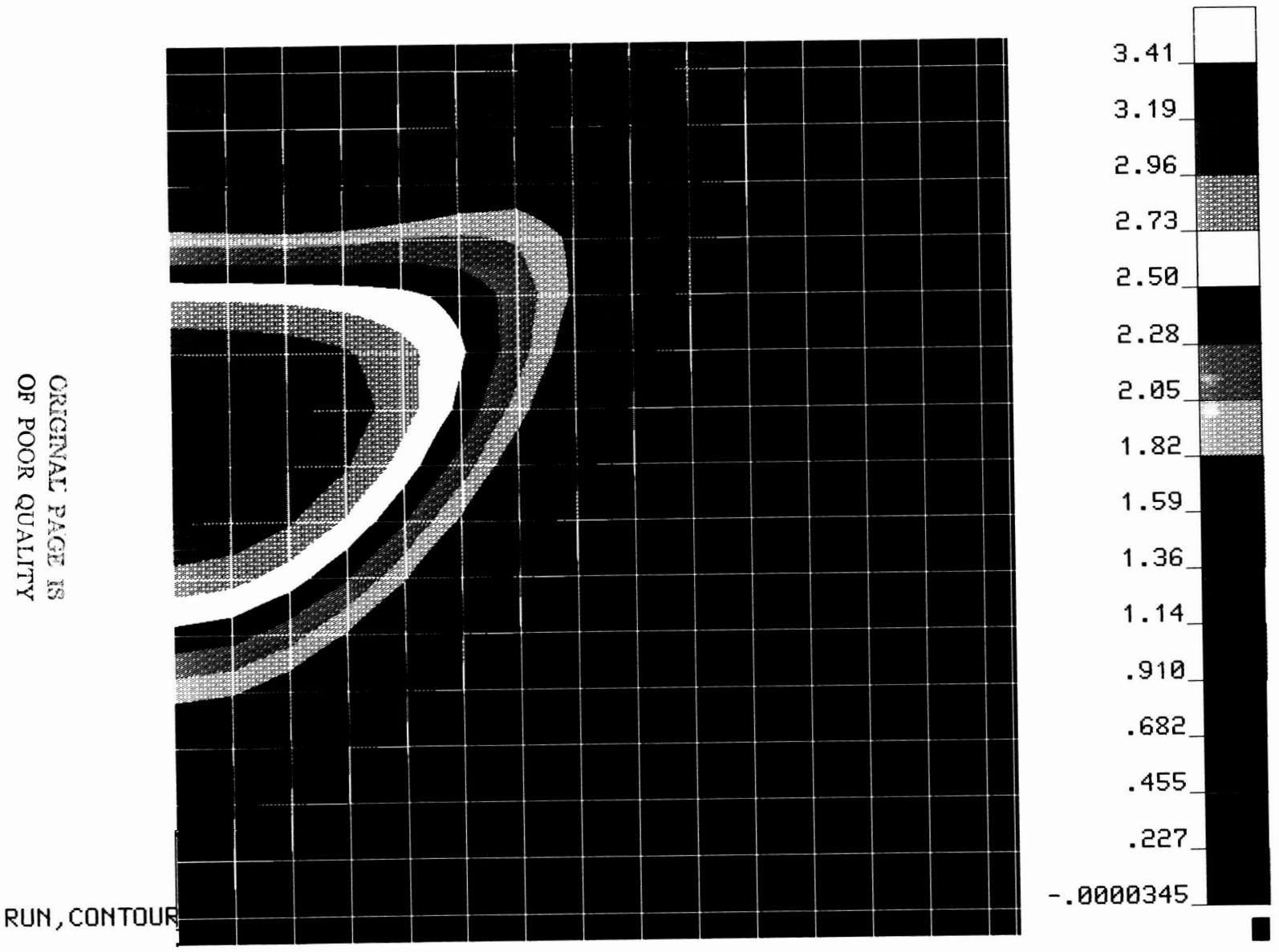

Figure II-3: Supersaturation Profile at 15 seconds

DISTRIBUTION LIST

Copy No.	
1 - 3	Dr. Joseph A. Nuth, III Code 691 NASA Goddard Space Flight Center Greenbelt, MD 20771
4 - 5*	NASA Scientific and Technical Information Facility P.O. Box 8757 Baltimore/Washington International Airport Baltimore, MD 21240
6	Dr. L. U. Lilleleht, CHE
7	Dr. E. L. Gaden, CHE, Chr.
8 - 9	Ms. E. H. Pancake, Clark Hall
10	SEAS Publications Files

* Reproducible copies

JO# 0752:vsh

UNIVERSITY OF VIRGINIA
School of Engineering and Applied Science

The University of Virginia's School of Engineering and Applied Science has an undergraduate enrollment of approximately 1,500 students with a graduate enrollment of approximately 560. There are 150 faculty members, a majority of whom conduct research in addition to teaching.

Research is a vital part of the educational program and interests parallel academic specialties. These range from the classical engineering disciplines of Chemical, Civil, Electrical, and Mechanical and Aerospace to newer, more specialized fields of Biomedical Engineering, Systems Engineering, Materials Science, Nuclear Engineering and Engineering Physics, Applied Mathematics and Computer Science. Within these disciplines there are well equipped laboratories for conducting highly specialized research. All departments offer the doctorate; Biomedical and Materials Science grant only graduate degrees. In addition, courses in the humanities are offered within the School.

The University of Virginia (which includes approximately 2,000 faculty and a total of full-time student enrollment of about 16,400), also offers professional degrees under the schools of Architecture, Law, Medicine, Nursing, Commerce, Business Administration, and Education. In addition, the College of Arts and Sciences houses departments of Mathematics, Physics, Chemistry and others relevant to the engineering research program. The School of Engineering and Applied Science is an integral part of this University community which provides opportunities for interdisciplinary work in pursuit of the basic goals of education, research, and public service.